CO Adsorption on MgO Thin-Films: Formation and Interaction of Surface Charged Defects

Support Information

Raphael da Silva Alvim[1,2*], Itamar Borges Jr.[3], Rita Maria Brito Alves[1]
Rodrigo B. Capaz[4,5] and Alexandre Amaral Leitão[2]

[1]*Departamento de Engenharia Química, Escola Politécnica, Universidade de São Paulo (USP), São Paulo, SP, 05508-900, Brazil.*
[2]*Departamento de Química, Instituto de Ciências Exatas, Universidade Federal de Juiz de Fora (UFJF), Juiz de Fora, MG, 36036-330, Brazil.*
[3]*Departamento de Química, Instituto Militar de Engenharia (IME), Rio de Janeiro, RJ, 22290-270, Brazil.*
[4]*Instituto de Física, Universidade Federal do Rio de Janeiro, Rio de Janeiro, RJ, 21941-972, Brazil.*
[5]*Brazilian Nanotechnology National Laboratory (LNNano), Brazilian Center for Research in Energy and Materials (CNPEM), Campinas, SP, 13083-100, Brazil.*

October 4, 2023

*raphael.alvim@usp.br

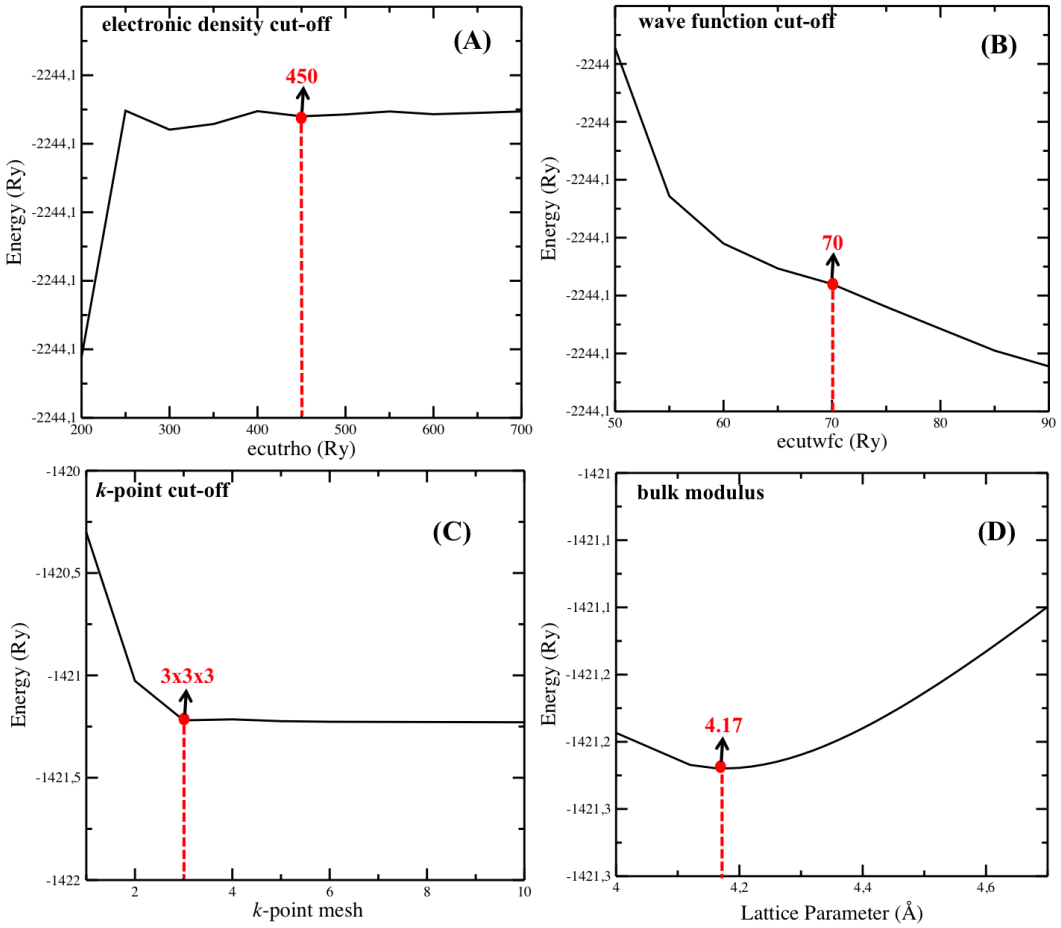

Figure-SI 1: Convergence tests calculated for cut-off energies of (A) the electronic densities and (B) the wave functions, (C) *k*-point mesh in First Brillouin-Zone (FBZ), and (D) bulk modulus with Murnaghan equation of state for the non-magnetic conductor Ag bulk.

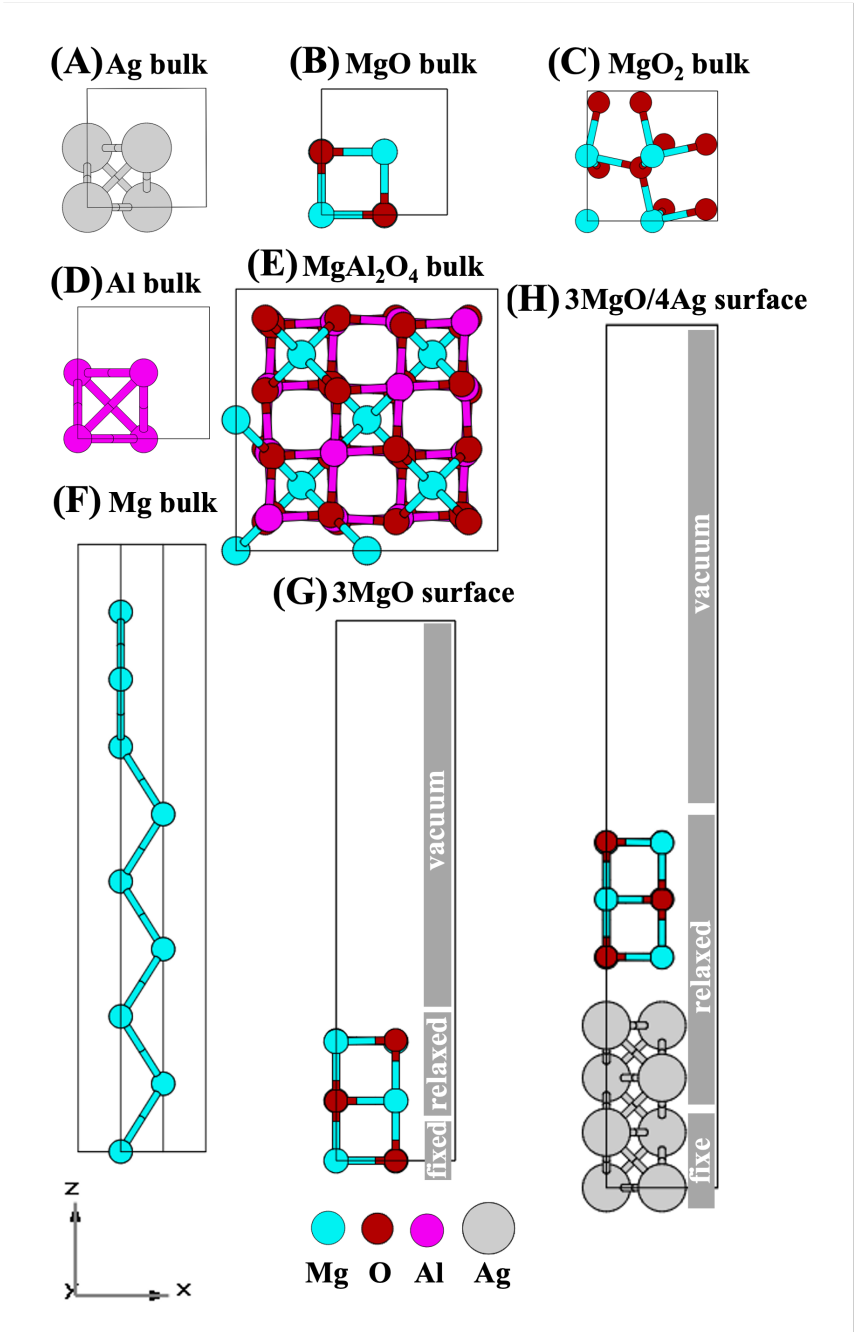

Figure-SI 2: Structural diagrams calculated for the (A) Ag, (B) MgO, (C) MgO_2, (D) Al, (E) $MgAl_2O_4$ and (F) Mg bulks, and the (G) unsupported MgO(001) and (H) supported MgO(001) 1×1 surfaces with 3 monolayers (ML) of MgO and 4 ML of Ag. The fixed, relaxed and vacuum regions in the surface models are showed. All structures are in a lateral vision. The structural parameters are in Table-SI 1.

Table-SI 1: Structural parameters of the Ag, MgO, MgO_2, Al, and Mg bulks, and the 1×1 cells for the unsupported and supported MgO(001) surfaces calculated with PBE functional and spin-polarized.

	Bulks						Surfaces (001)	
	Ag	**MgO**	**MgO_2**	**Al**	**$MgAl_2O_4$**	**Mg**	**3MgO**	**3MgO/4Ag**
Space Group	$Fm\bar{3}m$	$Fm\bar{3}m$	$Pa\bar{3}$	$Fm\bar{3}m$	$Fd\bar{3}m$	$R\bar{3}m$	$Fm\bar{3}m$	$Fm\bar{3}m$
Structural Parameters								
a (Å)	4.17	4.24	4.88	4.03	8.16	3.19	4.24	4.17
b (Å)	4.17	4.24	4.88	4.03	8.16	3.19	4.24	4.17
c (Å)	4.17	4.24	4.88	4.03	8.16	22.76	19.24	24.17
α (°)	90.00	90.00	90.00	90.00	90.00	90.00	90.00	90.00
β (°)	90.00	90.00	90.00	90.00	90.00	90.00	90.00	90.00
γ (°)	90.00	90.00	90.00	90.00	90.00	120.00	90.00	90.00

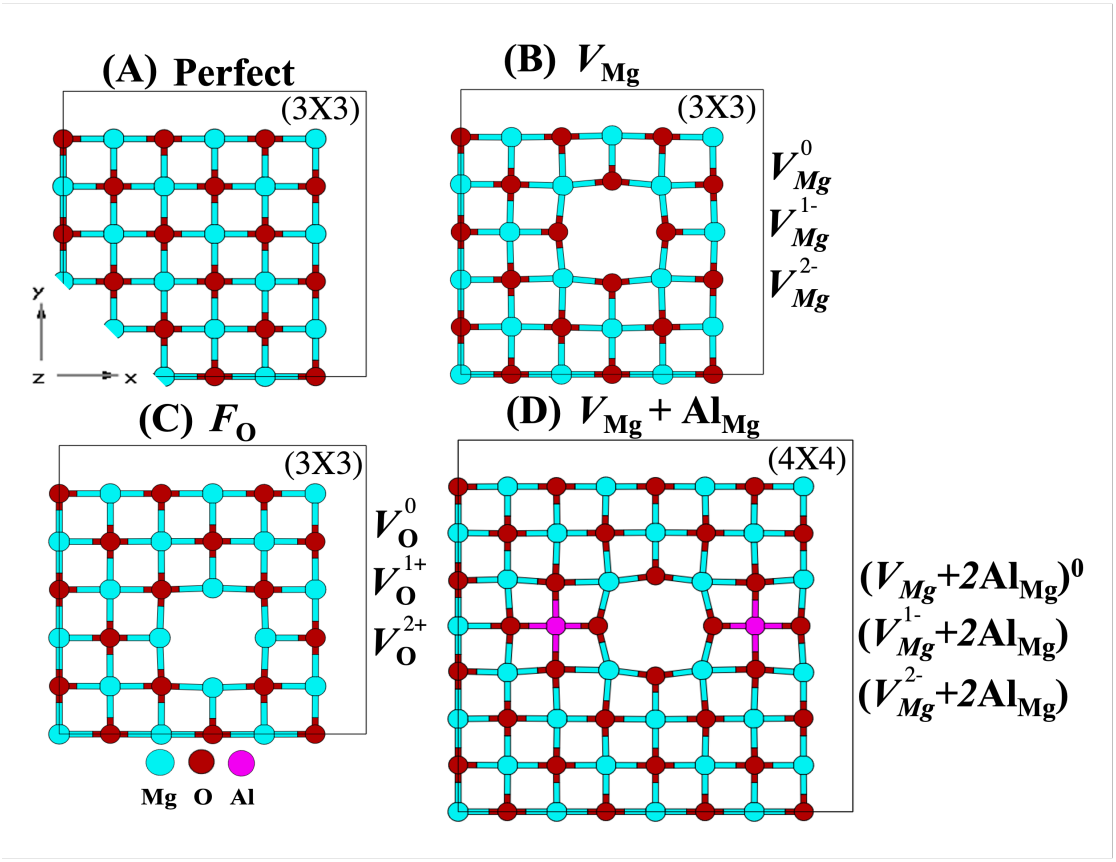

Figure-SI 3: Top view diagrams on the optimized supercells (3×3) and (4×4) calculated for the (A) perfect, and vacancies of: (B) Mg (V_{Mg}), (C) O (V_O), and (D) Mg + Al-doping $(V_{Mg}+2Al_{Mg})^0$ at both unsupported and supported MgO(001) surfaces with 3 monolayers (ML) of MgO and 4ML of Ag. The surface Mg^{2+} and O^{2-} ions move in different directions with respect to the center of the vacancy. For the paramagnetic Mg neutral vacancy (V_{Mg}^0), additional electrons were included with the charged states of paramagnetic 1- (V_{Mg}^{1-}) and diamagnetic 2- (V_{Mg}^{2-}). In the case of the diamagnetic O neutral vacancy (V_O^0), electrons missing (or holes) were considered with the states of paramagnetic 1+ (V_O^{1+}) and diamagnetic 2+ (V_O^{2+}). We considered also that the F_O^0 center is characterized for having a paramagnetic state (singlet), whereas the diamagnetic one (triplet) is energetically less stable at the 3MgO(001) and isoenergetic at the 3MgO(001)/4Ag(001) surfaces. Even as the Mg vacancy, we calculate for the Al-doping the Mg neutral vacancy $(V_{Mg}+2Al_{Mg})^0$, and the charged states of 1- $(V_{Mg}^{1-}+2Al_{Mg})$ and 2- $(V_{Mg}^{2-}+2Al_{Mg})$.

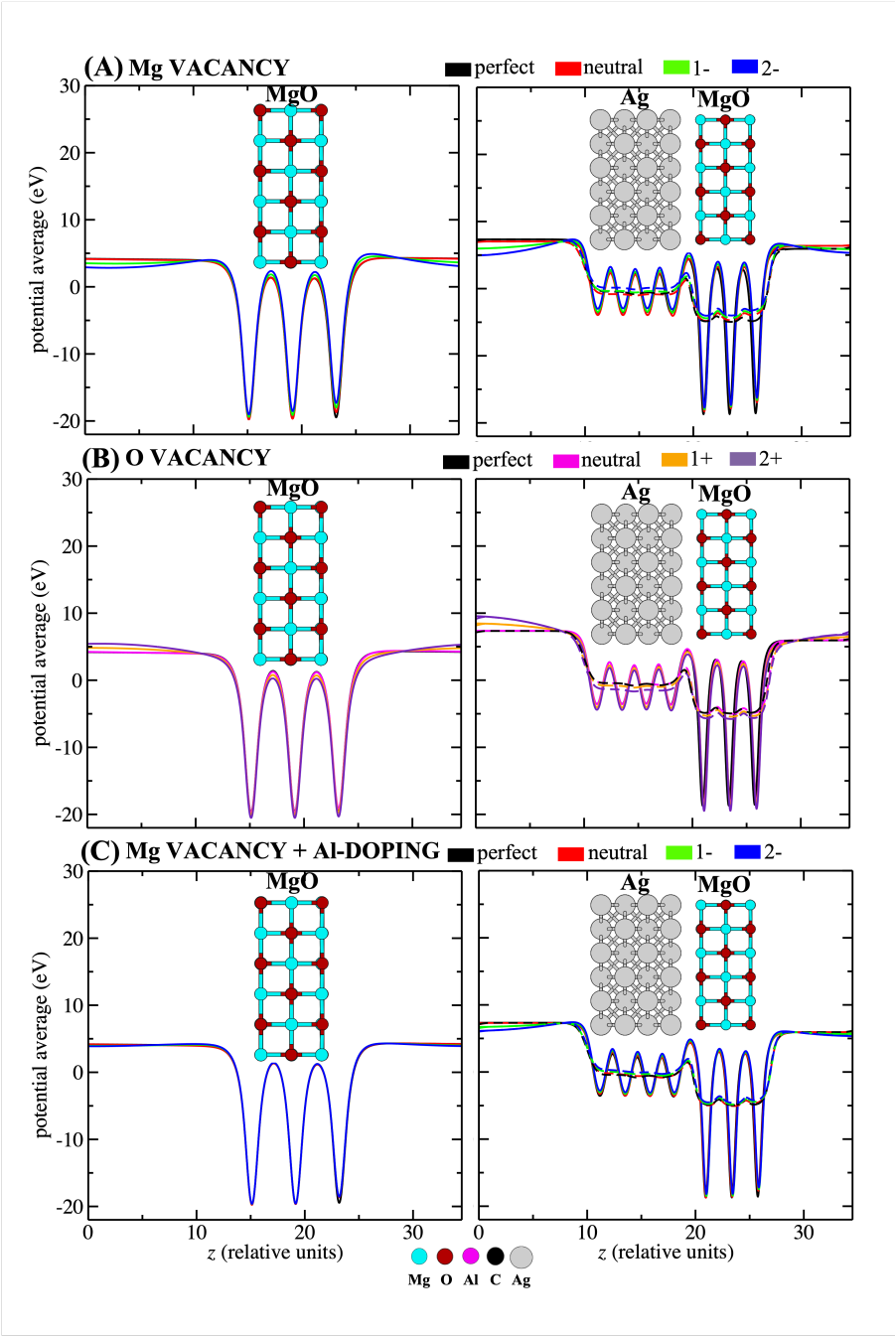

Figure-SI 4: Total electrostatic potential energy averages (Hartree) in the xy plane (planar) computed for the 3MgO(001) and 3MgO(001)/4Ag(001) surfaces with the neutral and charged vacancies of: (A) Mg (V_{Mg}), (B) O (V_{O}), and (C) Mg + Al-doping $(V_{\mathrm{Mg}}+2\mathrm{Al}_{\mathrm{Mg}})^{0}$. The one-dimensional (macroscopic) averages, taken over one interplanar distance, are also shown for the 3MgO(001)/4Ag(001) surfaces, where the effect of the presence of an uniform compensating background charge over the macroscopic electric dipole in the slab was reduced by introducing an artificial electric double layer in the vacuum region. For correcting the potential alignment, the value of the difference between the planar average in the middle of the charged 3MgO(001) and 3MgO(001)/4Ag(001) surfaces with respect to the neutral one can be used. All slabs were moved to the box center for better visualization.

The transition energy $\epsilon(q/q', w)_{S,L_z}$ between charge states q and q' of a certain defect is defined by Wang, D. et al. *Phys. Rev. Lett.* **2015**, *114*, 196801, as follows:

$$\epsilon(q/q')_{S,L_z} + \epsilon_{VBM} = \frac{\Delta E_{tot}(q, S, L_z) - \Delta E_{tot}(q', S, L_z)}{q' - q} \tag{1}$$

where $\Delta E_{tot}(q, S, L_z) = \Delta E^0_{tot} + \frac{\alpha' q^2}{\sqrt{S}} + \frac{\beta' q^2}{S}(L_z - L^0_z)$. Therefore, Equation (1) can be rewrite as follows:

$$\begin{aligned} \epsilon(q/q')_{S,L_z} + \epsilon_{VBM} = \frac{\Delta E^0_{tot}(q) - \Delta E^0_{tot}(q')}{q' - q} + \\ \frac{[\frac{\alpha'}{\sqrt{S}} + \frac{\beta'}{S}(L_z - L^0_z)](q^2 - q'^2)}{q' - q} \end{aligned} \tag{2}$$

Since energy corrections due to supercell Coulomb interactions should scale as q^2, we propose that α and β should have the following dependence on q and q':

$$\begin{aligned} \alpha &= \frac{\alpha'(q^2 - q'^2)}{q' - q} \\ \beta &= \frac{\beta'(q^2 - q'^2)}{q' - q} \end{aligned} \tag{3}$$

where the values of α', β', and L^0_z do not change regardless charge state, for a same type of defect. We assume that α' and β' do not depend on the specific type of defect, but only on the slab composition (MgO or MgO/Ag), which indeed would affect screening. Hence, $\epsilon(q/q')_0$ does not depend on S and L_Z in any transition.

$$\epsilon(q/q')_0 + \epsilon_{VBM} = \frac{\Delta E^0_{tot}(q) - \Delta E^0_{tot}(q')}{q' - q} \tag{4}$$

This allows us to reduce the number of DFT calculations needed to determine α and β for all defects. Therefore, α', β', and L^0_Z were calculated only for the L_Z and S variations in the MgO and MgO/Ag slabs from the $(0, 1-)$ transition in V_{Mg} (Figure-SI 5). So, we use the α, β, and L^0_Z values to obtain $\epsilon(q/q')_0$ for all charge state transitions in all defects at the MgO and MgO/Ag surfaces.

$$\begin{aligned}\epsilon(q/q')_{S,L_z} &= \epsilon(q/q^{'})_0 + \frac{\alpha}{\sqrt{S}} + \frac{\beta}{S}(L_z - L_z^0) \\ &= \epsilon(q/q^{'})_0 + \frac{\alpha}{\sqrt{S}} + \frac{\beta L_z}{S} - \frac{C}{S}\end{aligned} \tag{5}$$

where $C = \beta L_z^0$ and $\epsilon(q/q^{'})_0$ is the "true" transition energy.

For the MgO and MgO/Ag slabs, the values calculated for $\epsilon(q/q^{'})_0$ are shown in Table-SI 2. These values were then used to move the curves of formation energy (ΔE^q_{for}(defect) in Equation (1) in main text) so that the transitions of the charge states match the calculated $\epsilon(q/q^{'})_0$.

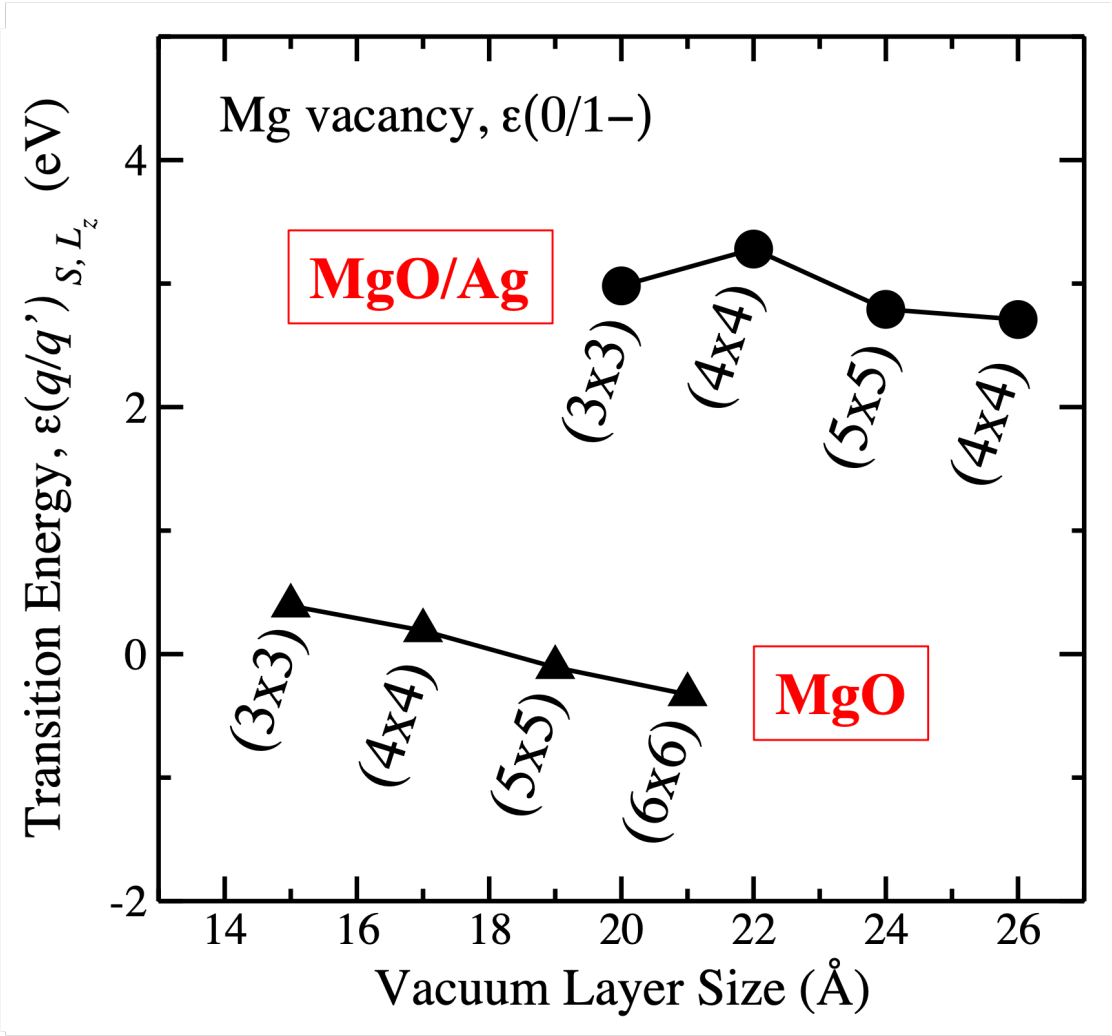

Figure-SI 5: Curves of transition energy ($\epsilon(q/q')_{S,L_z}$) for the transition of charge $\epsilon(0/1-)$ through different supercell sizes: (3×3), (4×4), (5×5) and (6×6) for the MgO slab (triangle); and (3×3), (4×4) and (5×5) for the 3MgO/4Ag slab (circle). The vacuum layer size was also increased. The terms of total energy of the slabs of vacancy with charge q and q' ($\Delta E_{tot}(q, \text{vacancy})$ and $\Delta E_{tot}(q', \text{vacancy})$) were obtained without further optimization of the surfaces.

Table-SI 2: Values of $\epsilon(q/q^{'})_0$ in eV calculated for each transition of charge state in the vacancies of Mg (V_{Mg}), O (V_{O}), and Mg + Al-doping (V_{Mg}+2$\mathrm{Al}_{\mathrm{Mg}}$)^0.

		$\epsilon(q/q^{'})_0$ **(eV)**	
Defect	**Charge Transition**	MgO	MgO/Ag
V_{Mg}	$(0,1-)$	1.36	0.35
	$(1-,2-)$	6.69	4.73
V_{O}	$(2+,1+)$	-6.68	-7.89
	$(1+,0)$	-1.67	0.38
(V_{Mg}+2$\mathrm{Al}_{\mathrm{Mg}}$)^0	$(0,1-)$	3.76	0.58
	$(1-,2-)$	7.67	2.42

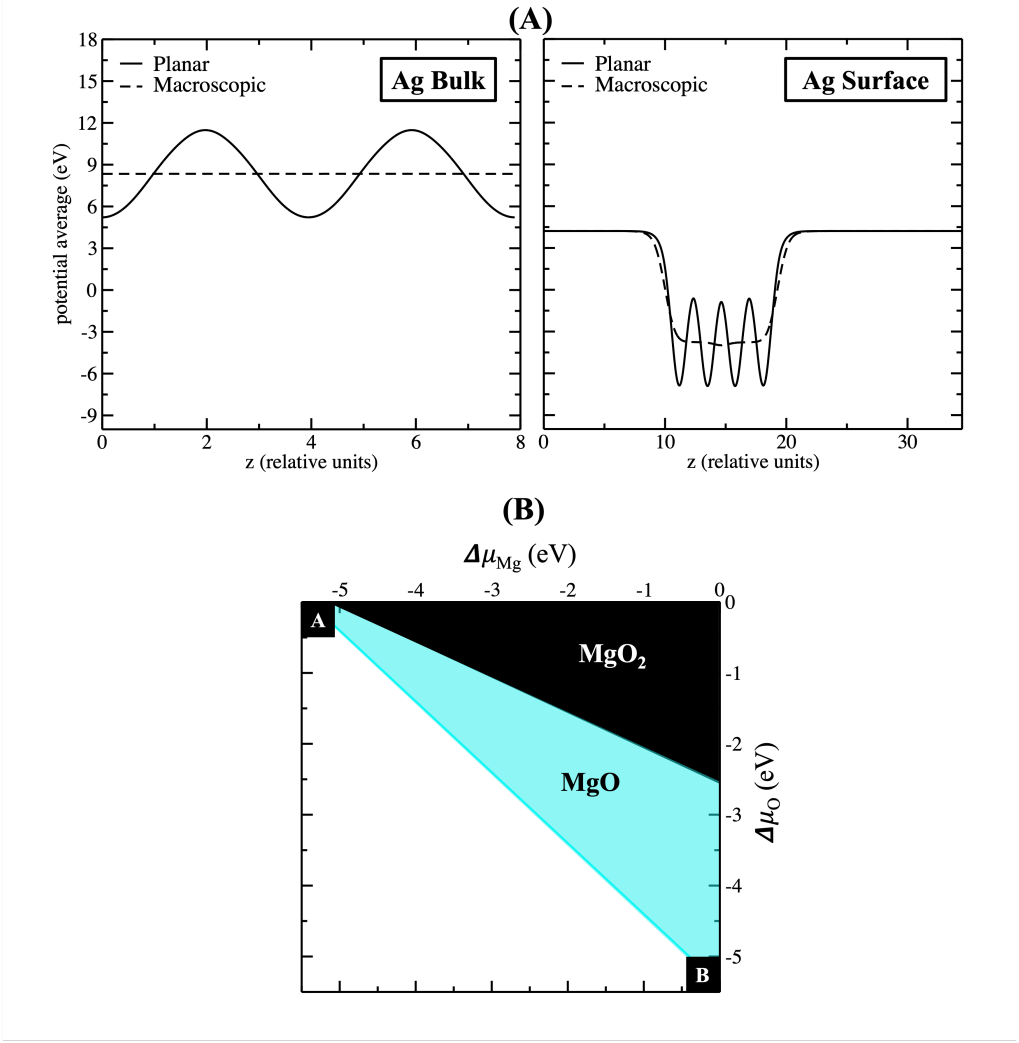

Figure-SI 6: (A) Total electrostatic potential energy averages (Hartree) in the xy plane (planar) computed for the the Ag bulk and the 4Ag(001) surface. The one-dimension (macroscopic) averages are also showed, where it was reduced by introducing an artificial electric double layer in the vacuum region. The slab was moved to the box center for better visualization. (B) Phase diagram calculated for the formation of the elemental bulk phases of the magnesium oxide (MgO) and magnesium peroxide (MgO_2) under the range of the $\Delta\mu_{Mg}$ and $\Delta\mu_{O_2}$ chemical potentials between the O-rich ($\Delta\mu_{O_2}$=0) and Mg-rich ($\Delta\mu_{Mg}$=0) conditions as indicated by labels A and B, respectively.

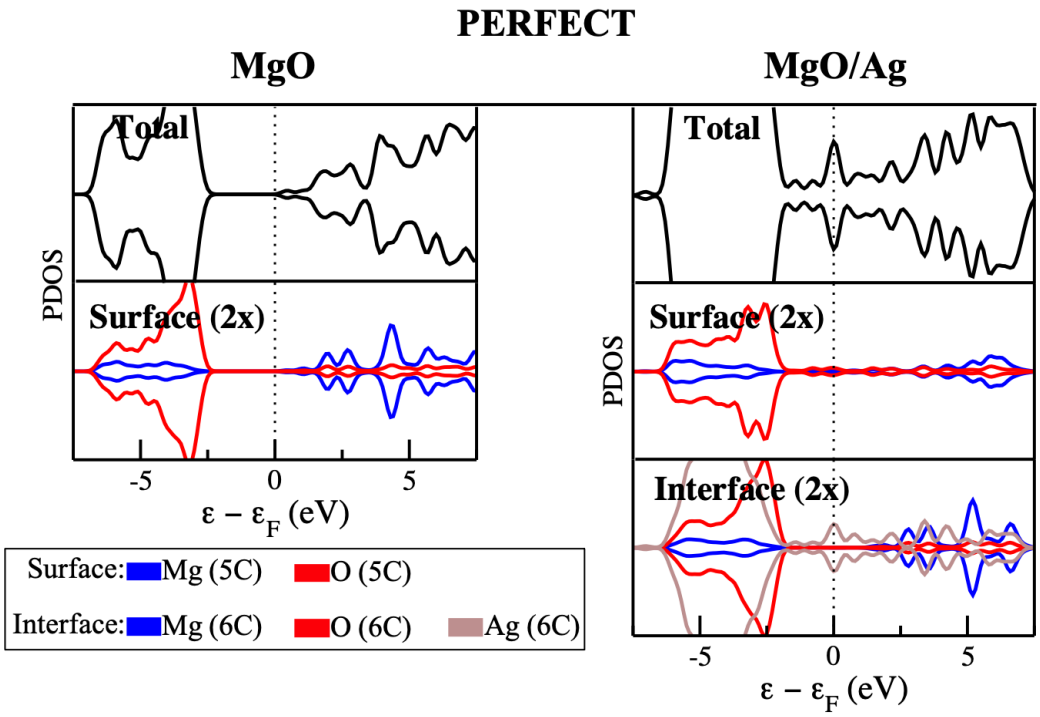

Figure-SI 7: Projected density of states (PDOS) calculated for the slabs of the perfect 3MgO(001) and 3MgO(001)/4Ag(001) surfaces. For the thin-film, we also accounted the MgO/Ag interface. Mg (5C) and O (5C) represent the five-coordinated Mg and O sites at the surface, respectively; while Mg (6C), O (6C) and Ag (6C) represent the six-coordinated Mg, O, and Ag sites at the interface, respectively.